EBioMedicine 44 (2019) 86–97

Contents lists available at ScienceDirect

EBioMedicine

journal homepage: www.ebiomedicine.com

EBioMedicine
Published by THE LANCET

p16^{INK4A}-expressing mesenchymal stromal cells restore the senescence–clearance–regeneration sequence that is impaired in chronic muscle inflammation

Takako S. Chikenji *, Yuki Saito, Naoto Konari, Masako Nakano, Yuka Mizue, Miho Otani, Mineko Fujimiya

Department of Anatomy, Sapporo Medical University School of Medicine, Sapporo, Hokkaido 060-8556, Japan

ARTICLE INFO

Article history:
Received 4 January 2019
Received in revised form 28 April 2019
Accepted 6 May 2019
Available online 23 May 2019

Keywords:
Mesenchymal stromal cell
Regenerative medicine
Tissue remodelling
Senescence
Chronic inflammation

ABSTRACT

Background: The therapeutic benefits of mesenchymal stromal cells (MSCs) include treatment of chronic inflammation. However, given the short-lived engraftment of these cells *in vivo*, their therapeutic efficacy remains mysterious. Transient induction of cellular senescence contributes to activation of immune cells, which promotes clearance of damaged cells during tissue remodelling. This may occur in tissue-resident mesenchymal progenitor cells during regeneration. Elucidation of the role of senescence in tissue-resident mesenchymal progenitor cells during regeneration would provide insight into the profile of therapeutic MSCs for treatment of chronic inflammatory disease.

Methods: We evaluated multipotent mesenchymal progenitor cells, termed fibro/adipogenic progenitors (FAPs), and immune cells in acute muscle injury (AMI) model mice and mice with myosin-induced experimental autoimmune myositis, a model of chronic inflammatory myopathy (CIM). Human bone marrow MSCs were optimised for the treatment of CIM using placental extract.

Finding: FAPs in AMI transiently expressed p16^{INK4A} on days 1 and 2 after injury and recruited phagocytic immune cells, whereas in CIM, p16^{INK4A} expression in FAPs was low. Cellular senescence occurs during the natural maturation of the placenta. Therefore, we used human placental extract to induce p16^{INK4A} expression in therapeutic human bone marrow MSCs in culture. Treatment of CIM with p16^{INK4A}-expressing MSCs promoted tissue remodelling by transiently increasing the abundance of engrafted MSCs, inducing cellular senescence in innate FAPs, and recruiting phagocytic immune cells.

Interpretation: MSCs may exert their effect by remodelling the chronic inflammatory environment *via* senescence-related regenerative processes.

© 2019 The Authors. Published by Elsevier B.V. This is an open access article under the CC BY-NC-ND license (http://creativecommons.org/licenses/by-nc-nd/4.0/).

1. Introduction

Mesenchymal stromal cells (MSCs) have attracted a great deal of attention as a novel therapeutic for use against multiple chronic inflammatory diseases. Due to their potent immunosuppressive and anti-inflammatory activities, availability, and genomic stability during *in vitro* expansion, therapies based on these cells have been rapidly brought to clinical trials, and the number of such trials increases yearly [1]. However, the lack of proven mechanisms and plausible explanatory hypotheses for the benefits conferred by MSCs can no longer be ignored by researchers seeking to develop safe and effective therapies [2]. Several biomarkers, including tumour necrosis factor (TNF)–stimulated gene 6 protein (TSG-6) and indoleamine 2,3-dioxygenase (IDO) [3], have been reported as markers of MSC function; however, it is widely believed that MSCs are not solely responsible for immunomodulation, and that other cells such as macrophages or regulatory T cells are also involved in immunosuppressive activities [4,5]. In addition, the supporting evidence for MSC efficacy has been met with skepticism because of the short-lived engraftment of MSCs *in vivo* [2].

In a demonstration of the efficacy of short-lived MSC engraftment, Galleu et al. reported that MSCs are induced to undergo perforin-dependent apoptosis by recipient cytotoxic cells, and that this process is important for initiation of MSC-induced immunosuppression [6]. Cell death is a crucial step for tissue regeneration during inflammation [7]. In muscle regeneration, apoptosis of multipotent mesenchymal progenitor cells, termed fibro/adipogenic progenitors (FAPs), is required during the remodelling process associated with acute inflammation, and increases survival of FAPs due to failure of apoptosis, which results in muscle fibrosis [8]. However, the regulatory mechanisms that govern

* Corresponding author.
E-mail address: chikenji@sapmed.ac.jp (T.S. Chikenji).

https://doi.org/10.1016/j.ebiom.2019.05.012
2352-3964/© 2019 The Authors. Published by Elsevier B.V. This is an open access article under the CC BY-NC-ND license (http://creativecommons.org/licenses/by-nc-nd/4.0/).

Research in context

Evidence before this study

The therapeutic benefits of mesenchymal stromal cells (MSCs) are well documented, but given the short-lived engraftment of these cells *in vivo*, currently no plausible hypotheses can explain their therapeutic efficacy. Transient induction of cellular senescence contributes to cell clearance, followed by tissue remodelling.

Added value of this study

Here, we show that placental extracts induced $p16^{INK4A}$ expression in therapeutic MSCs. Cellular senescence occurs during the natural maturation program of the placenta. Treatment of chronic inflammatory myopathy (CIM) mice with $p16^{INK4A}$-expressing MSCs promoted tissue remodelling by transiently increasing the abundance of engrafted MSCs, inducing cellular senescence in innate fibro/adipogenic progenitors (FAPs), and recruiting phagocytic immune cells. This phenomenon was similar to the endogenous regeneration process after acute damage to skeletal muscle.

Implications of all the available evidence

MSCs may exert their effect by remodelling the chronic inflammatory environment *via* senescence-related regenerative processes.

these properties of MSCs, specifically in regard to their ability to modify tissue homeostasis and inflammation by producing various cytokines and growth factors, remain unknown.

Cellular senescence is another mechanism that leads to cell elimination. In contrast to cells that undergo apoptosis, senescent cells enter a cell-cycle arrest and persist in the tissue. Subsequently, they influence neighbouring cells by secreting soluble factors, a response collectively known as the senescence-associated secretory phenotype (SASP), which activates immune cells to promote clearance of cell debris during tissue remodelling [9]. The importance of senescent cells is highlighted by the fact that cellular clearance and interference with the phagocyte switch from an inflammatory to a pro-regenerative phenotype have positive effects on the outcome of tissue regeneration [9,10].

The tumour suppressor proteins $p16^{INK4A}$ and $p14/p19^{ARF}$, which are encoded by the *CDKN2A* locus, are often transcriptionally activated in cells undergoing senescence; moreover, these factors are major regulators of the senescence program [11]. Although $p16^{INK4A}$ expression increases with age or chronic inflammation/fibrosis, and is a robust senescence marker in multiple human and mouse tissues [12,13], $p16^{INK4A}$-expressing cells also play essential roles in wound healing [14,15] and suppression of liver fibrosis in adults [10]. Senescent cells have acute beneficial roles when present during repair or in the context of cancer, but their chronic effects include promotion of tumour progression and contribute to the pathology of age-related diseases [16]. That is, the breakdown of normal senescence mechanisms that promote tissue remodelling worsens the deleterious effects of these cells in chronic inflammatory pathogenesis, suggesting that targeting senescent cells is a therapeutic option for ameliorating disease progression or chronic inflammation.

Idiopathic inflammatory myopathies are rare, heterogeneous, autoimmune diseases characterised by muscle weakness, inflammation, and fibrosis [17]. The pathogenic mechanism of these myopathies is unknown, but autoimmune processes are strongly implicated [17]. We hypothesise that (1) if breakdown of the senescence mechanism underlies the pathogenesis of chronic inflammatory myopathies, it could result in accumulation of heterogeneous cell types, specifically in chronic inflammation but not in acute inflammation; and (2) if cellular senescence is observed in acute inflammation, it may promote regenerative inflammation in chronic inflammatory myopathies.

In this study, we observed transient, high-level expression of $p16^{INK4A}$ in FAPs in the early phase of a mouse model of acute inflammatory injury. FAPs promoted immune cell infiltration with distinct temporal and spatial kinetics over the course of muscle regeneration. By contrast, these cellular dynamics broke down in a mouse model of chronic inflammatory myopathy, in which FAPs expressed low levels of $p16^{INK4A}$. The inherent cellular senescence mechanism of mesenchymal cells, which promote muscle regeneration, may explain the efficacy of MSC therapy against chronic inflammatory disease. Furthermore, we developed $p16^{INK4A}$-expressing MSCs as a supplemental therapy for chronic inflammatory myopathy. This approach increased therapeutic efficacy by inducing FAP senescence and orchestrating immune cellular dynamics by recruiting macrophages, neutrophils, and natural killer (NK) cells, which collectively constitute the regenerative environment of acute muscle injury in chronic inflammatory myopathy.

2. Materials and methods

2.1. Animals

Mice were maintained in a specific pathogen–free facility. All animal care and experiments were performed in accordance with protocols approved by the Ethics Committee of the Animal Experimentation Center of the Sapporo Medical University School of Medicine. Female BALB/c mice (>6 weeks of age; Sankyo Lab Service, Tokyo, Japan) were used in the experiments.

2.2. Muscle injury model

Isoflurane was used to anesthetise the mice. The acute muscle injury (AMI) model was created by injecting 50 μl of 1.2% barium chloride (Sigma-Aldrich, St. Louis, MO, USA) diluted in sterile distilled water into the triceps surae as previously described [18]. The chronic inflammatory myopathy (CIM) model used to study autoimmune myopathy was created by immunising mice with partially purified myosin, including myosin-binding protein C. The myosin was partially purified as reported previously [19], with slight modifications. Briefly, skeletal muscle obtained from 8 to 10-week-old BALB/c mice was stored at −80 °C until use. Thawed and minced muscle (30 g) was washed four times in 0.03 M KCl/0.15 M sodium phosphate buffer (pH 7.5), 1 mM EDTA, and 1 mM DTT. Myosin was extracted by incubation of 30 g muscle with 90 ml chilled 0.3 M KCl/0.15 M phosphate buffer containing 5 mM $MgCl_2$, 5 mM ATP, 1 mM DTT, and 1 mM EDTA on ice for 45 min with constant agitation. The homogenate was centrifuged for 30 min at 4 °C at 2200*g*. For myosin precipitation, the supernatant was collected, filtered, and diluted with 15 volumes of chilled ultrapure water. The precipitate was recovered *via* centrifugation for 10 min at 4 °C at 10,000*g*, dissolved in 0.5 M KCl, and stored at −80 °C. BALB/c mice (8 weeks old) were each immunised three times, at 1-week intervals, with 200 μl of an emulsion containing 1 mg myosin with 100 μg complete Freund's adjuvant (Chondrex Inc., Redmond, WA, USA), which was injected bilaterally into the hock (first immunisation) [20], tail base (second immunisation), and flank (third immunisation). One hour after the first immunisation, pertussis toxin (500 ng in 100 μl saline; List Biological Laboratories, Campbell, CA, USA) was intraperitoneally injected into each animal.

2.3. Cell preparation and flow cytometry

Triceps surae muscles were carefully dissected to remove attached fat tissue, blood vessels, tendons, and nerves. Muscles were dissociated

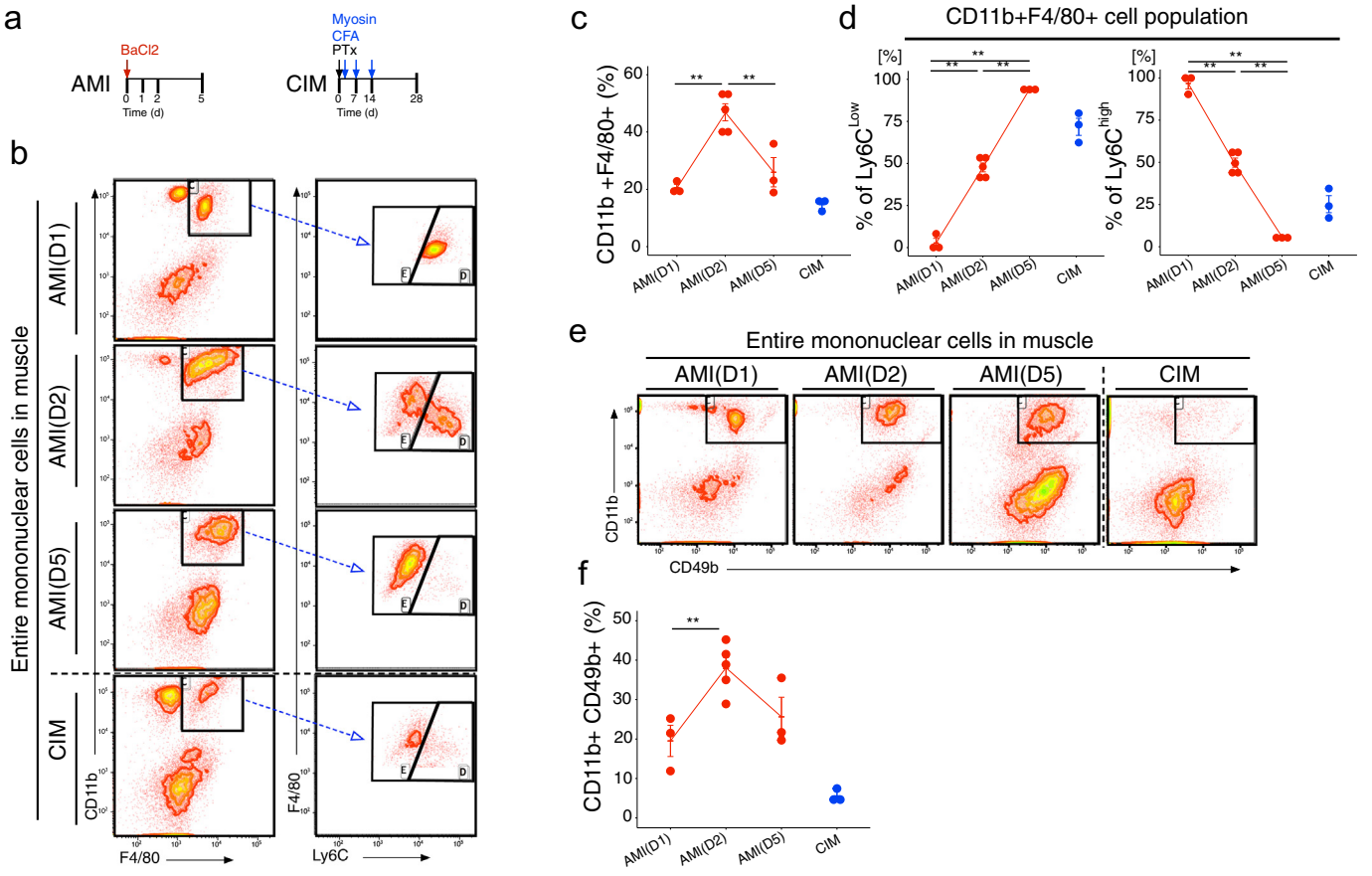

Fig. 1. Activation of pro-inflammatory and phagocytic cells is impaired in chronic inflammatory myopathy. (a) Schematic diagram of procedures for generating the acute muscle injury (AMI) and chronic inflammatory myopathy (CIM) models. (b) Representative CD11b, F4/80, and Ly6C counter plots for CIM and AMI (1, 2, and 5 days after injury). (c and d) Percentages of CD11b + F4/80+ macrophages (c), CD11b + F4/80 Ly6Clow anti-inflammatory macrophages (d), and CD11b + F4/80 Ly6Chi pro-inflammatory macrophages (d). (e) Representative CD11b and CD49b counter plot in CIM and AMI (1, 2, and 5 days after injury). (f) Percentage of CD11b + CD49b NK cells. Quantitative data are shown as means ± SEM with dot plots. *P*-values were determined by one-way ANOVA adjusted by Tukey's method. (*$P < .05$, **$P < .001$).

mechanically and digested for 60 min at 37 °C in PBS containing 2.5 mM $CaCl_2$ and 0.2% collagenase type 2 (Worthington Biochemical Corporation, Lakewood, NJ, USA). The muscle tissue was passed several times through an 18-gauge needle and digested for 30 min at 37 °C. The resultant muscle slurries were filtered twice, first through a 100-μm cell strainer (EASYstrainer™ Cell, Greiner Bio-One, Kremsmuenster, Austria) and then through a 40-μm cell strainer (Greiner Bio-One). Erythrocytes were removed by treatment of the sample with RBC lysis solution (QIAGEN, Hilden, Germany). The isolated cells were stained for 15 min in Zombie Violet™ Dye (BioLegend, San Diego, CA, USA) diluted 1:100 in PBS, washed, and then fixed and permeabilised with the PerFix-nc Kit (Beckman Coulter, Brea, CA, USA) for detection of intracellular antigen. Antibody concentrations and sources are shown in Supplementary Table 1. Negative controls were stained with isotype control or secondary antibody only. Flow cytometry analysis was performed on a FACSCanto™ II system (BD Biosciences, Franklin Lakes, NJ, USA) equipped with 405-, 488-, and 633-nm lasers. The FACSDiva™ (BD Biosciences) and Kaluza V1.5a (Beckman Coulter) software were used to collect and analyse the data. A representative example of identification of dead cells with Zombie Violet™ Dye and gating strategies is depicted in Fig. S1.

2.4. Ethics statement

The ethical committees of Sapporo Medical University approved this study (Reference number, 262–110, 302–1134). Human placenta and bone marrow samples were collected after written informed consent was obtained from all donors.

2.5. Human mesenchymal stromal cells (MSCs) and placental extract (PE) preparations

Heparinised bone marrow (10 ml) was aspirated from the iliac crest during total hip arthroplasty procedures. All donors were diagnosed with osteoarthritis of the hip joint. Each sample was centrifuged at 300*g* for 10 min. The cell fraction was isolated and suspended in an amount of complete medium (Dulbecco's modified Eagle's medium [DMEM; Sigma-Aldrich], containing 4500 mg/l glucose, 10% fetal bovine serum [FBS], and 1% penicillin–streptomycin)) equal in volume to the originally aspirated bone marrow. Suspended bone marrow cells (1 ml) were plated in a 100-mm polystyrene culture dish in 9 ml of complete medium. Cultures were maintained at 37 °C in a humidified atmosphere containing 5% CO_2. Nonadherent cells were removed after 1 week of adhesion, and the culture medium was replaced twice a week. MSCs were harvested as passage 0 after 3–4 weeks of culture. After trypsinisation, 4×10^5 MSCs were seeded in 100-mm polystyrene culture dishes in 9 ml of complete medium (passage 1). At passage 2, MSCs were cultured with complete medium (MSCs) or medium supplemented with PE (MSCs+PE) *in vitro* during 48–72 h. Continuous cultivation (CC) of MSCs was performed from passages 6 to 11. MSC and MSC + PE samples were labelled with PKH26 (Sigma-Aldrich) before treatment *in vivo*. Then, 1×10^5 PKH-labelled MSCs or MSCs+PE were suspended in 25 μl PBS and locally injected into the triceps surae of each leg. Cells were tested for mycoplasma using the e-Myco™ Mycoplasma PCR Detection Kit (iNtRON Biotechnology, Inc., Seongnam-si, South Korea).

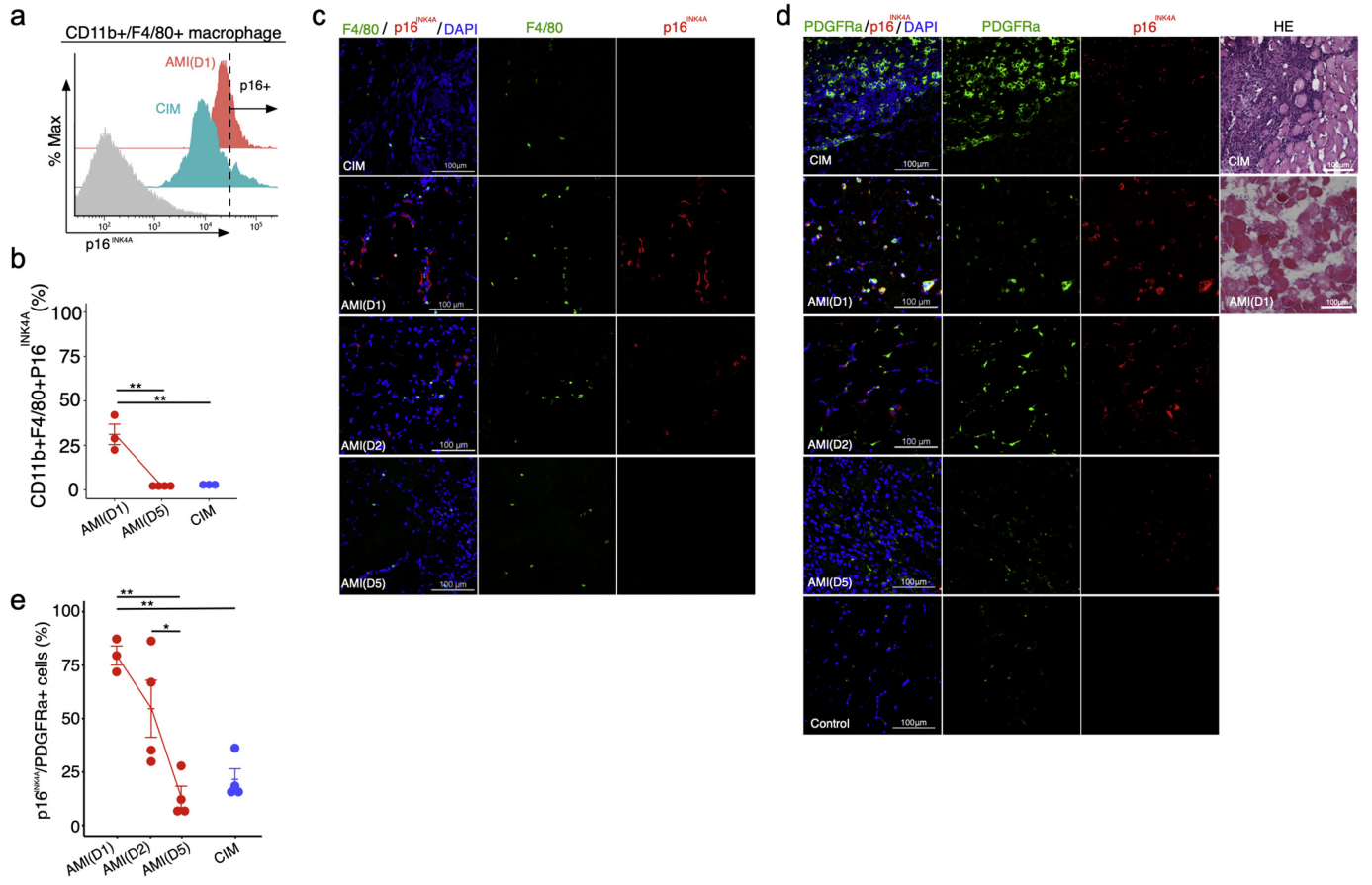

Fig. 2. PDGFRα-positive fibro-adipogenic progenitors (FAPs) express high levels of $p16^{INK4A}$ in acute muscle injury. (a and b) Flow cytometry analysis of CD11b, F4/80, and $p16^{INK4A}$, and percentages of CD11b + F4/80+ $p16^{INK4A}$+ cells in both AMI and CIM ($n = 3$ per group). (c) Representative image of F4/80- and $p16^{INK4A}$- immunostained triceps surae in CIM and AMI (1, 2, and 5 days after injury). (d and e) Representative image of hematoxylin and eosin (H&E) staining and PDGFRα- and $p16^{INK4A}$- immunostained triceps surae in CIM and AMI (1, 2, and 5 days after injury) and Control (d), and percentage of $p16^{INK4A}$+ FAPs in randomly chosen fields of view (n = 3–4 per group) (e). Quantitative data are shown as means ± SEM (dot plot). P-values were determined by one-way ANOVA, adjusted by Tukey's method. (*P < .05, **P < .001).

After removal of RBCs from minced placental tissue, the tissue was suspended in serum-free medium and shaken for 48–72 h at 4 °C. After centrifugation, supernatants of tissue suspensions were obtained as PE. Protein concentrations were determined using a BCA assay kit (Thermo Fisher Scientific, Waltham, MA, USA).

2.6. Histology and immunofluorescence

Triceps surae muscles were frozen in liquid nitrogen–cooled isopentane and stored at −80 °C until analysis. Cryosections (8 μm thick) obtained on a cryostat were air-dried, fixed in 4% paraformaldehyde, washed in PBS, and either stained with hematoxylin & eosin or immunostained. For immunostaining, tissue sections were incubated in 0.3% Triton-X/0.01 M PBS (PBS-T) and incubated with 2% bovine serum albumin for 60 min at room temperature (RT). After 0.01 M PBS-T washes, the sections were incubated at 4 °C overnight with primary antibodies, and then with secondary antibodies. Antibody concentrations and sources are shown in Supplementary Table 1.

For immunohistochemistry of cultured cells, the cells were grown on 8-well Lab-Tek™ chamber slides (Thermo Scientific™ Nunc™; Thermo Fisher Scientific). The cultured cells were fixed in 4% paraformaldehyde for 15 min at RT, washed in PBS-T, and incubated with 2% bovine serum albumin for 60 min at RT. After PBS-T washes, the cells were incubated at 4 °C overnight with primary antibodies, followed by secondary antibody staining. Antibody concentrations and sources are shown in Supplementary Table 1. Secondary antibodies were coupled to fluorochromes (Cyanine Dye 3, Alexa Fluor 488, or Alexa Fluor 647), and nuclei were stained with 1:1000 4′,6-diamidino-2-phenylindole (DAPI) (D523, Dojindo, Kumamoto, Japan). After further washes, tissue sections were mounted in VECTASHIELD (Vector Laboratories, Burlingame, CA, USA). Sections were examined under a confocal laser scanning microscope (Nikon/A1; Nikon, Tokyo, Japan).

2.7. SA-β-gal assay

SA-β-gal assays were conducted using the Senescence Detection Kit (BioVision, Inc., Milpitas, CA, USA). Briefly, cells were cultured on 8-well chamber slides for 48 h with or without PE. Cultured cells were fixed for 15 min at RT in 4% paraformaldehyde and then incubated overnight at 37 °C in SA-β-gal buffer. After washes, the cells were analysed under a microscope.

2.8. Cell proliferation assay

MSCs and MSCs+PE were cultured on 96-well culture plates at a concentration of 2×10^3 cells per well in DMEM supplemented with 10% FBS and 1% penicillin/streptomycin. After culturing for 24 h and 72 h, a cell proliferation assay was performed using the Cell Counting Kit-8 (Dojindo).

2.9. Co-Culture of MSCs with Macrophages

MSCs and MSCs+PE were labelled with PKH26 (Sigma-Aldrich), and RAW264.7 macrophages were labelled with PKH2 (Sigma-Aldrich). Co-

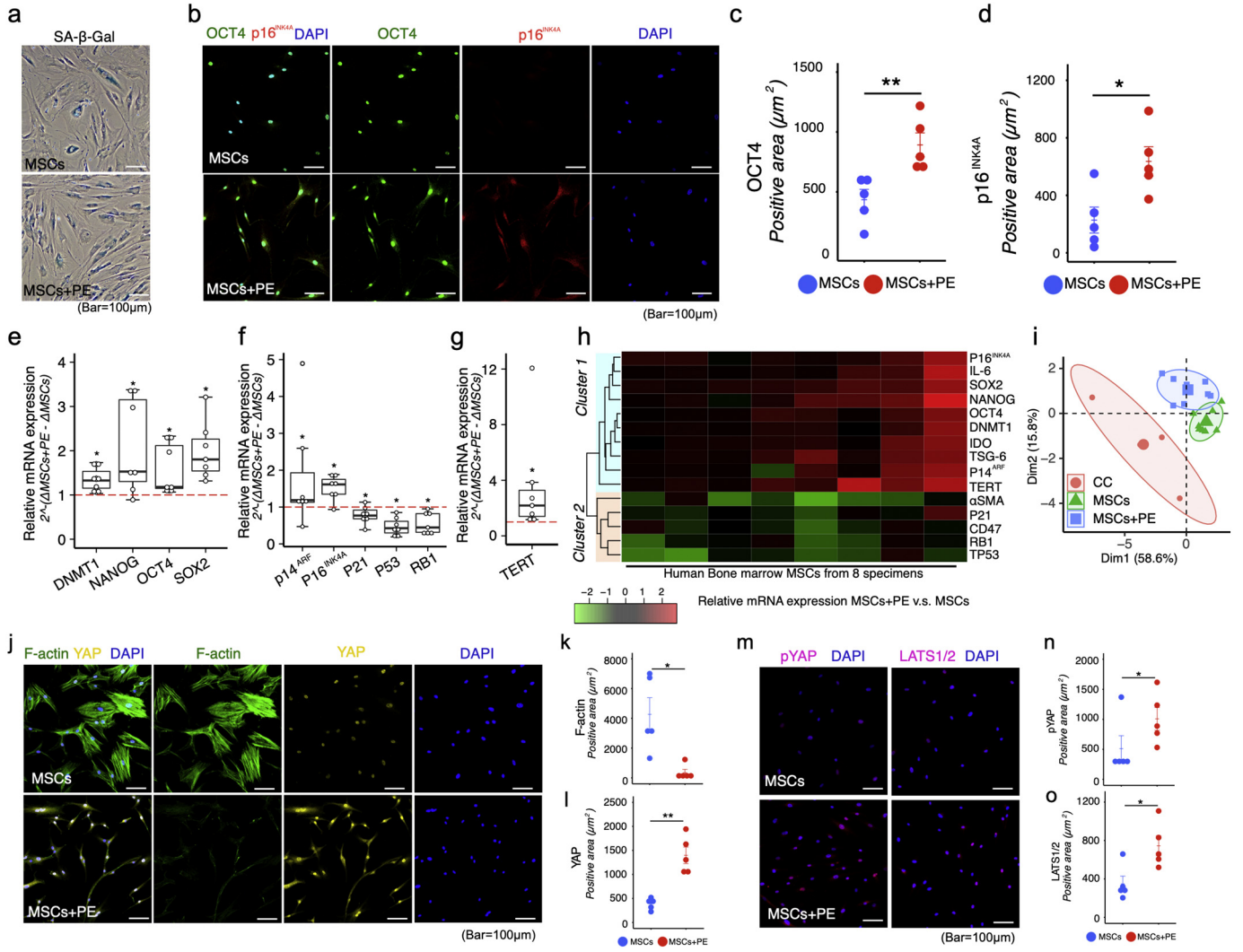

Fig. 3. Placental extract (PE) induces functional senescence in MSCs. (a) Representative image of SA-β-galactosidase in MSCs with or without PE supplementation *in vitro*. (b–d) Representative confocal images of MSCs immunostained for OCT4 and $p16^{INK4A}$ with or without PE supplementation *in vitro* (b), and quantitation of OCT4- and $p16^{INK4A}$-positive area ($n = 5$ per group) (c and d). (e–g) Relative mRNA expression of *DNMT1*, *NANOG*, *OCT4(POU5F1)*, *SOX2*, $p14^{ARF}$(*CDKN2A*), $p16^{INK4A}$(*CDKN2A*), *p21*(*CDKN1A*), *p53*(*TP53*), and *RB1*, and *TERT* in MSCs+PE ($n = 7$ per group). Dashed line indicates mRNA expression in MSCs without PE supplementation. (h) Hierarchical clustering of stemness-, senescence-, and cytokine-related gene expression in MSCs ($n = 8$). Red indicates up-regulation and green indicates down-regulation by PE supplementation. (i) Principal component analysis (PCA) of stemness-, senescence-, and cytokine-related gene expression in MSCs (n = 8), MSCs+PE (n = 8), and continuously cultivated (CC) MSCs ($n = 4$). (j–o) Representative image of confocal images of F-actin, Yap, phospho-Yap (p-Yap), and LATS1/2 immunostained MSCs with or without PE supplementation *in vitro*, and quantitation of F-actin–, Yap-, phospho-Yap (p-Yap)–, and LATS1/2-positive areas (n = 5 per group). Quantitative data are shown as means ± SEM (dot plot) or means and medians with interquartile range (IQR) and 1.5× IQR (box-and-whisker plot). P-values were determined by two-tailed Student's *t*-test. (*P < .05, **P < .001).

culture was performed using a double-chamber co-culture system with a 0.4-μm pore size membrane (12-well insert, BD Biosciences) separating the upper and lower chamber cells. MSCs (2×10^4 cells/well) were placed in the upper chamber, and RAW264.7 cells (2×10^5 cells/well) in the lower chamber. The co-cultures were incubated for 24 h, and then MSCs or MSCs+PE cells were collected by trypsinisation. The collected MSCs (2×10^4 cells/well) were co-cultured above the RAW264.7 macrophages in complete medium for 48 h. Cells were tested for mycoplasma using the e-Myco™ Mycoplasma PCR Detection Kit (iNtRON Biotechnology, Inc., Seongnam-si, South Korea). After trypsinisation, cells were collected and analysed on a FACSCanto™ II (BD Biosciences), equipped with 488-nm and 633-nm lasers, to detect double-positive staining. Data collection and analysis were conducted using FACSDiva™ (BD Biosciences) and Kaluza V1.5a (Beckman Coulter).

2.10. RNA extraction and quantitative real-time PCR

Total RNA, isolated from cultured MSCs using the TRI Reagent® (Molecular Research Center, Inc., Cincinnati, OH, USA), was reverse-transcribed into cDNA using the Omniscript RT Kit (205,113; QIAGEN). Quantitative PCR was performed using Power SYBR® Green Master Mix (4,368,702; Applied Biosystems, Foster City, CA, USA) in a 7500 Real-Time PCR System (Applied Biosystems) and the following conditions: 50 °C for 2 min, 95 °C for 10 min, and 40 amplification cycles comprising 95 °C for 15 s and 60 °C for 1 min. Expression levels were normalised against the corresponding levels of *GAPDH* and *18S rRNA* mRNA. The primer sequences used for the PCR are shown in Supplementary Table 2. Samples were compared using the ΔΔCt method.

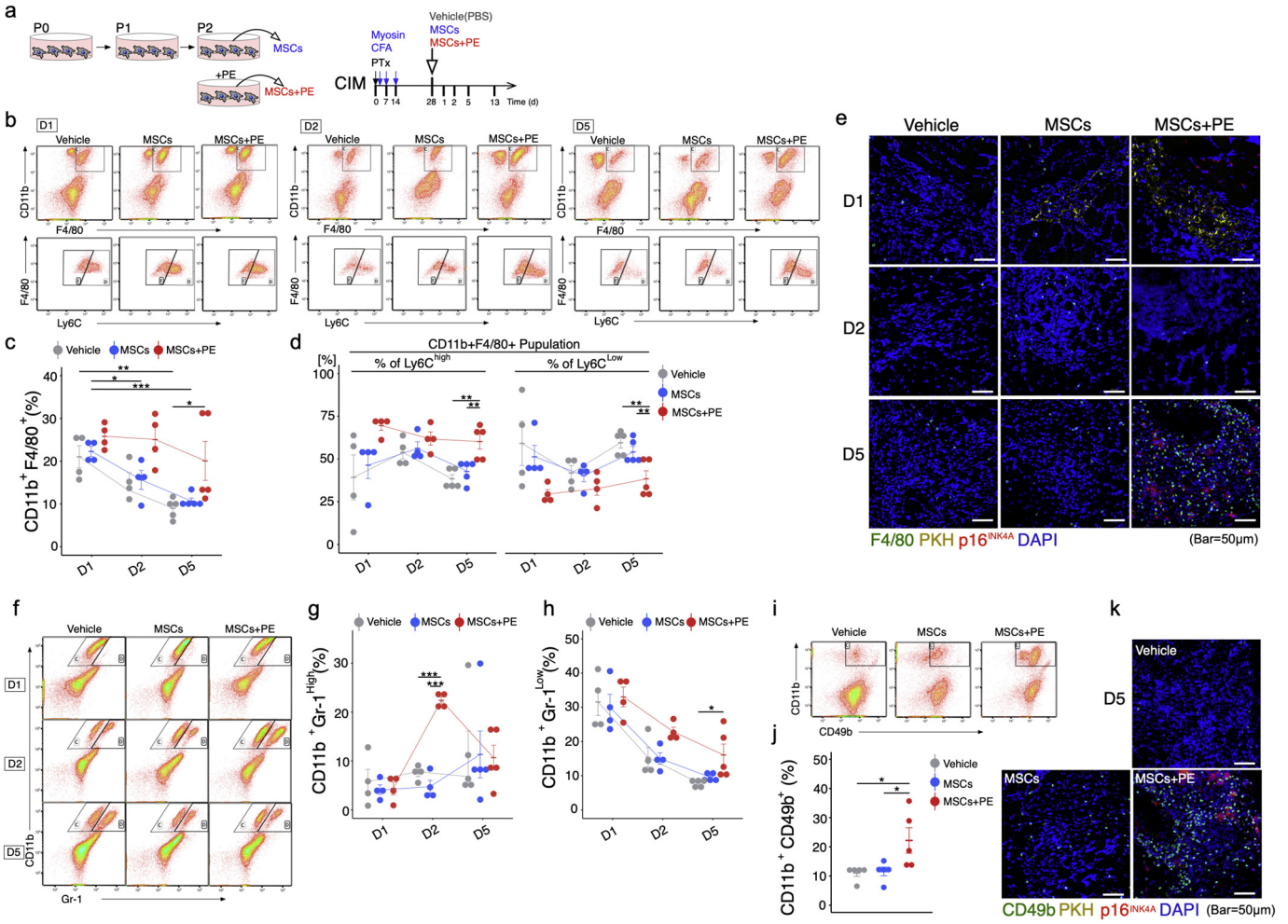

Fig. 4. MSCs + PE exert therapeutic effects on CIM muscle *via* immuno-activation. (a) Protocol for treatment of CIM mice using MSCs with or without PE supplementation. (b) Detection of the macrophage phenotype switch in CIM 1, 2, and 5 days after MSC treatment. (c-d) Percentage of CD11b + F4/80+ (total) macrophages (c), CD11b + F4/80+ Ly6Chi pro-inflammatory macrophages (d), and CD11b + F4/80+ Ly6Clow pro-fibrosis macrophages (d) (n = 4 per group). (e) Representative confocal images of F4/80- and $p16^{INK4A}$-immunostained triceps surae in CIM 1, 2, and 3 days after injection of PKH-labelled MSCs. (f–j) Flow cytometry analysis of CD11b and Gr-1 (Neutrophil) (f), and CD11b and CD49 (NK cell) (i), and quantification following MSC treatment (g, h, and j). (k) Representative confocal images of CD49b- and $p16^{INK4A}$-immunostained triceps surae in CIM 5 days after injection of PKH-labelled MSCs. Quantitative data are shown as means ± SEM (dot plot). P-values were determined by one-way ANOVA adjusted by Tukey's method. (*P < .05, **P < .001).

2.11. Array analysis for cytokines

DMEM +10% FBS + PE, and DMEM +10% FBS samples containing protein and supernatant cytokines from MSC cultures, with or without PE, were analysed using the Proteome Profiler™ Array Human XL Cytokine Array Kit (ARY022B; R&D Systems, Minneapolis, MN, USA).

2.12. CRISPR knockout in MSCs

CDKN2A knockout was performed using the p14 ARF/p16 CRISPR/Cas9 KO plasmid (Santa Cruz Biotechnology, Dallas, TX, USA), which includes green fluorescent protein (GFP) and a pool of three plasmids, each encoding Cas9 nuclease and a target-specific 20-nt guide RNA designed for maximum knockout efficiency. On day 1, MSCs were plated in 6-well plates in antibiotic-free growth medium. On day 2, the medium was replaced with fresh medium, and plasmid DNA and UltraCruz® transfection reagent complex were added (KO-MSC). The cells were incubated for 72 h at 37 °C, and transfection efficiency was confirmed by monitoring protein expression of GFP and p16INK4A by confocal laser scanning microscopy (Fig. S2). As a scrambled control, we used the Control CRISPR/Cas9 plasmid (sc-418,922) (SC-MSC). At passage 2, KO-MSCs or SC-MSCs were cultured with complete medium supplemented with PE *in vitro*. Then, 1×10^4 KO-MSCs or SC-MSCs were suspended in 25 μl PBS and locally injected into the triceps surae of each leg.

2.13. Statistical analysis

No power calculations were performed to determine required sample sizes. No specific randomisation method was used to determine the allocation of animals to experimental groups and their treatment. Mice were only excluded from the study if their health status was compromised, such as when they had visible wounds from fighting. Investigators were not blinded to allocations during the experiments or at the outcome assessment, except for behavioural assessments. Quantitative data are presented as either means ± the standard error of the mean (SEM) or median with interquartile range (IQR) and 1.5 × IQR. Dot plots or box-and-whisker plots were generated using ggplot2, a plotting system for R based on The Grammar of Graphics (The R Foundation for Statistical Computing, Vienna, Austria). The R packages FactoMineR and factoextra were used to generate heat maps, Ward's hierarchical agglomerative clustering, and principal component analyses. The normality of the data was checked using the Shapiro-Wilk test. A pairwise *t*-test was used for comparisons between two groups. One-way analysis of variance (ANOVA) was performed to determine differences among three or more groups. Pairwise comparisons were only performed when statistical significance was indicated by one-way ANOVA. Tukey's method was used to adjust *P*-values for multiple comparisons. All statistical analyses were conducted using EZR, a graphical user interface for R [21]. A two-sided *P*-value <.05 was considered statistically significant.

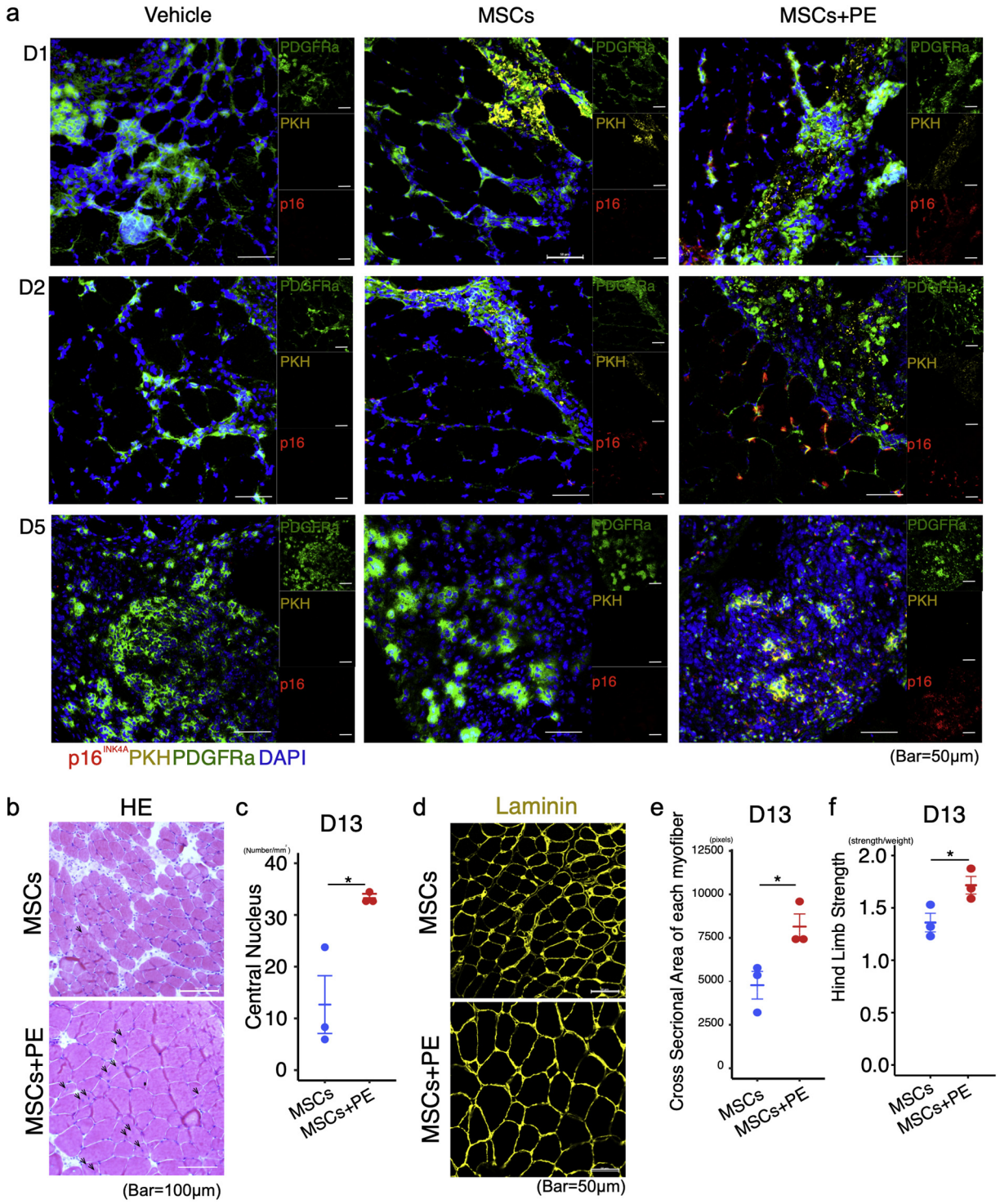

Fig. 5. MSCs + PE induce senescence in resident FAPs and improve muscle function. (a) Representative image of PDGFRα and $p16^{INK4A}$ staining of PKH-labelled MSC–transplanted muscle, 1, 2, and 5 days after MSC transplantation. (b and c) Representative image of H&E staining and quantification of the number of regenerating myofibers with central nuclei. (d-f) Representative image of laminin-immunostained triceps surae in CIM 13 days after MSC transplantation (d), quantification of cross-sectional area of each myofiber (e), and muscle function as evaluated by hindlimb grip strength test (f). Quantitative data are shown as means ± SEM (dot plot). P-values were determined by two-tailed Student's t-test. (*P < .05, **P < .001).

3. Results

3.1. Breakdown of immune cellular dynamics in chronic inflammatory myopathy

Acute muscle injury induces an orchestrated inflammatory process aimed at clearing damaged cells, coordinating the regenerative response, and restoring tissue homeostasis [22]. However, chronic inflammation interferes with this orchestration by promoting the accumulation of immune and mesenchymal cells [23], ultimately resulting in fibrosis. During efficient regeneration, granulocytes, monocytes, macrophages, fibroblasts, and FAPs transiently increase in number, and then subsequently become less abundant in order to create space for satellite cells, which promote myoblast proliferation and muscle regeneration [22].

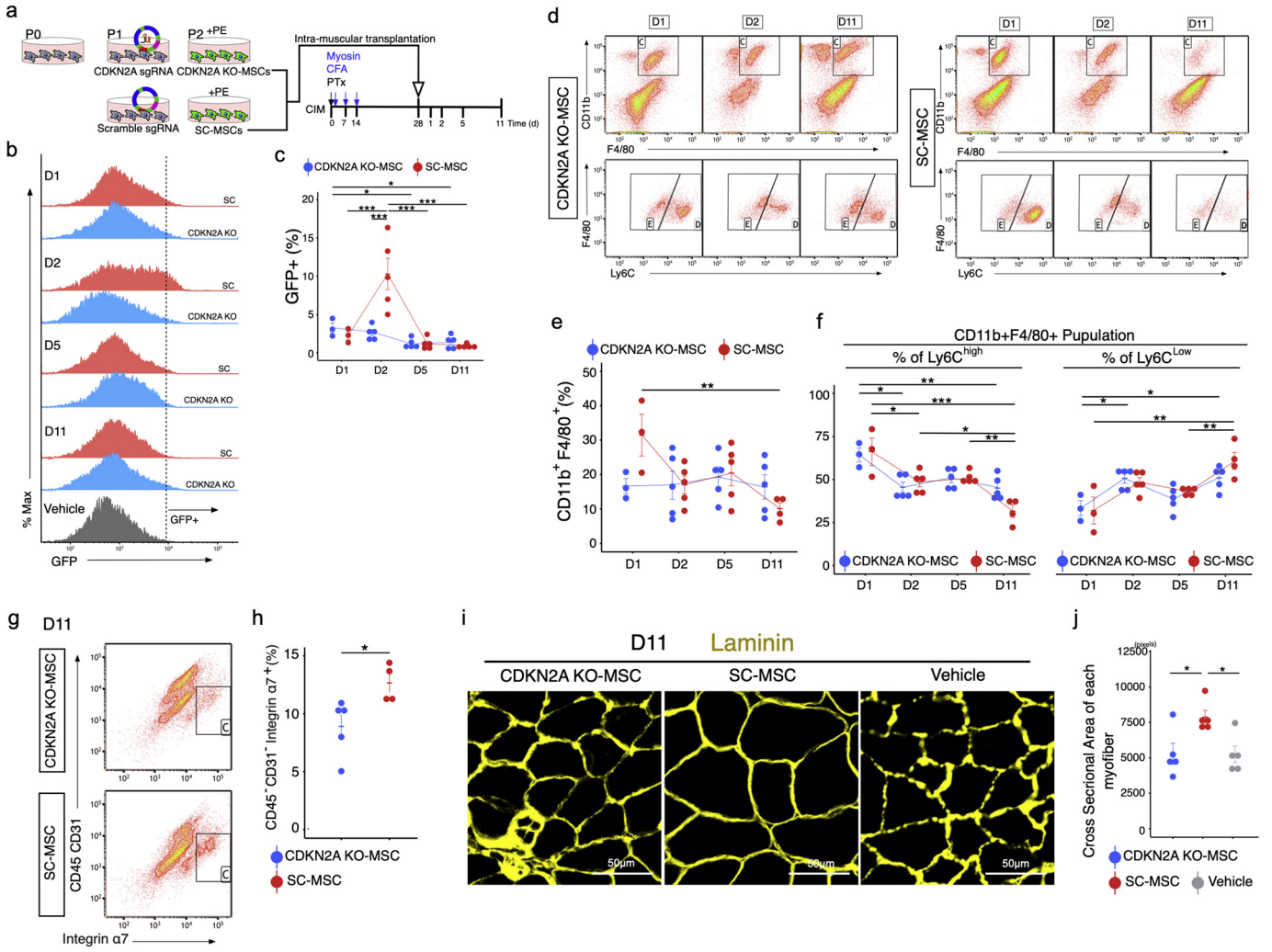

Fig. 6. CDKN2A-KO MSCs exert reduced therapeutic effects in CIM. (a) Procedure for generation of CDKN2A KO-MSCs and protocol for MSC treatment. (b and c) Flow cytometry analysis of GFP+ cells of triceps surae in CIM 1, 2, 5, and 11 days after transplantation of GFP-labelled MSCs (b), and percentage of GFP+ cells (c). (d–f) Flow cytometry analysis of CD11b, F4/80, and Ly6C (d); quantification following MSC transplantation: percentage of CD11b + F4/80+ total macrophages (e), CD11b + F4/80+ Ly6Chi pro-inflammatory macrophages (f), and CD11b + F4/80+ Ly6Clow pro-fibrotic macrophages (f) (n = 3–5 per group). (g and h) Flow cytometry analysis of CD45, CD31, and α7-integrin (g), and quantification 11 days after MSC transplantation (h) (n = 3–4 per group). (i and j) Representative image of laminin-immunostained triceps surae 11 days after MSC transplantation (i), and quantification of the cross-sectional area of each myofiber (j). Quantitative data are shown as means ± SEM (dot plot). P-values were determined by two-tailed Student's t-test or one-way ANOVA adjusted by Tukey's method. (*P < .05, **P < .001).

To investigate the difference in inflammatory cell switching between acute and chronic muscle inflammation, we used flow cytometry to measure the time-dependent change in the inflammatory cell population. For this purpose, we used two models: barium chloride–induced acute muscle injury (AMI) model mice [18], and mice with myosin-induced experimental autoimmune myositis as a model of chronic inflammatory myopathy (CIM) [19] (Fig. 1a). AMI model mice, which are induced by intra-muscular injection of barium chloride, regenerate muscle tissue over 3–4 weeks after acute inflammation [18]. The CIM model was created by immunising mice with partially purified myosin, including myosin-binding protein C, resulting in infiltration of $CD8^+$ and major histocompatibility complex (MHC) class I^+ cells (Fig. S3), as also occurs in polymyositis [19]. In AMI, the abundance of $CD11b^+$ $F4/80^+$ $Ly6C^{hi}$ monocytes/macrophages and $CD11b^+$ $CD49b^+$ NK cells, which are typical pro-inflammatory and phagocytic cells, increased from day 1 to day 2, and then declined rapidly on day 5 (Fig. 1b–f). On the other hand, in CIM, the levels of $CD11b^+$ $F4/80^+$ $Ly6C^{hi}$ monocyte/macrophages and $CD11b^+$ $CD49b^+$ NK cells remained low (Fig. 1b–f). Further, in AMI we observed $CD11b^+$ $F4/80^+$ $Ly6C^{hi}$ pro-inflammatory monocytes/macrophages switch to $CD11b^+$ $F4/80^+$ $Ly6C^{low}$ anti-inflammatory monocytes/macrophages, whereas in CIM the $CD11b^+$ $F4/80^+$ $Ly6C^{low}$ cells were predominant (Fig. 1b–f). These results indicated that the absence of pro-inflammatory and phagocytic cell activation is a hallmark of muscle degeneration in CIM. The switch from a pro-inflammatory to an anti-inflammatory phenotype is essential for clearance of cell debris and tissue regeneration [24,25]. Further, the anti-inflammatory phenotype of macrophages promotes fibroblast proliferation, which increases deposition of connective tissues [26]. We hypothesise that the failure of macrophages to undergo this phenotypic change is one of the mechanisms underlying muscle degeneration in chronic inflammation. The numbers of pro-inflammatory monocytes and macrophages in CIM were similar to those in early-stage AMI (days 1 and 2) (Fig. S4), but the abundance of anti-inflammatory monocyte/macrophages was elevated in CIM to levels comparable to those of AMI on day 5 (Fig. S4). In other words, in CIM, the balance of inflammatory *vs.* anti-inflammatory macrophages was unregulated in the chronic inflammatory environment. Therefore, we considered that the proportions of various immune cell populations could provide insight into the immune cell dynamics during acute and chronic inflammation.

Deficiency in $p16^{INK4A}$ influences macrophage polarisation in a manner that inhibits pro-inflammatory signalling by these cells [27]. Hence, we next investigated whether macrophages express $p16^{INK4A}$ after

muscle injury. Flow cytometry measurements of $p16^{INK4A}$ expression in $CD11b^+$ $F4/80^+$ macrophages in single-cell suspensions derived from muscle revealed that the percentage of $CD11b^+$ $F4/80^+$ $p16^{INK4A+}$ cells was higher in AMI on day 1 than in AMI on day 5 and in CIM (Fig. 2a and b). Immunohistochemical examination revealed that $F4/80^+$ macrophages expressed high levels of $p16^{INK4A}$ in AMI on days 1 and 2 (Fig. 2c); however, F4/80-negative interstitial cells expressed $p16^{INK4A}$ more frequently near $F4/80^+$ macrophages (Fig. 2c).

3.2. Transient senescent FAPs and macrophages are observed in acute muscle injury

FAPs are typical interstitial cells that act as key regulators of muscle inflammation by influencing immune cells, including macrophages [8]. Hence, to identify which cells undergo cellular senescence in the muscle interstitial space near macrophages, we investigated whether FAPs express $p16^{INK4A}$. Immunohistochemical examination revealed transient expression of $p16^{INK4A}$ in FAPs marked with platelet-derived growth factor receptor alpha (PDGFRα) after AMI induction, which gradually decreased and returned to the pre-induction level by day 5 (Fig. 2d and e). In CIM mice, $p16^{INK4A}$ expression in $PDGFR\alpha^+$ cells was significantly lower than on day 1 of AMI, and HE staining revealed large numbers of infiltrating cells and fibrotic regions (Fig. 2d and e). We also found that the proportion of FAPs that were $p16^{INK4A+}$ (79%) was higher than the proportion of macrophages that were $p16^{INK4A+}$ (31%) on day 1 in AMI, suggesting that the $PDGFR\alpha^+$ cells might be the primary cells that enter senescence under inflammatory conditions.

In summary, during the regenerative inflammation process associated with AMI, $p16^{INK4A+}$ senescence occurred strongly in $PDGFR\alpha^+$ cells at the early phase of injury, and the abundance of neighbouring immune cells transiently increased, and then decreased. In CIM, however, cellular senescence was rare among $PDGFR\alpha^+$ cells, but was still more prominent than in non-injured muscle. It is possible that if $p16^{INK4A+}$ expression could be induced in therapeutic MSCs, and these cells could be subsequently injected into a tissue exhibiting chronic inflammation consisting primarily of $p16^{INK4A}$-low $PDGFR\alpha^+$ cells, it might trigger a switch to the regenerative condition.

3.3. Generation of functional senescent mesenchymal stem cells using placental extract

We hypothesised that senescence of mesenchymal cells could promote a chronic inflammatory environment that promotes regeneration. To test this idea, we examined senescent human bone marrow MSCs conditioned *in vitro*. In MSCs, cellular senescence upon increasing culture passage is accompanied by expression of p53, p21, $p16^{INK4A}$, but continuously cultivated senescent MSCs lose self-renewal capacity and multi-lineage differentiation potential *in vitro*, decreasing their immune modulation activity and ultimately making them less effective for treating disease [28,29]. Therefore, we focused on a type of senescence that occurs in a physiologically programmed manner in adult organisms, in particular in placenta, in which cells undergo functional senescence as part of their natural maturation program [30]. This physiologically programmed senescence is associated with marked senescence-associated beta-galactosidase (SA-β-gal) activity and expression of the DNA damage response (DDR) markers and p16, p21, and p53 [30].

For these experiments, we first established a process for generating functional senescent MSCs using placental extract (PE). Proteome array analysis of PE (Fig. S5) revealed abundant RBP-4 (retinol binding protein) and DPP-4 (dipeptidyl peptidase 4), both of which can induce cellular senescence [31]. To determine whether PE could induce $p16^{INK4A}$ expression in human bone marrow MSCs, we supplemented MSCs with PE *in vitro*. $p16^{INK4A}$ expression increased dramatically in MSCs exposed to 0.1 mg/ml PE in the culture media (Fig. S6); accordingly, we used 0.1 mg/ml PE in our subsequent *in vitro* experiments. Both MSCs and MSCs+PE had the capacity to undergo multilineage differentiation, expressed MSC surface markers, and exhibited colony-forming capability (Fig. S7).

Cells positive for SA-β-gal, a well-characterised marker of senescence, were present in PE-treated MSC cultures (MSCs+PE) at passage 2 (Fig. 3a). Immunocytometry revealed that expression of $p16^{INK4A}$ and OCT4 was higher in the MSC + PE group than in the untreated donor-matched MSCs (Fig. 3b–d). Transcription of pluripotency genes, such as *OCT4(POU5F1)*, *SOX2*, and *NANOG*, which suppress cell differentiation and maintain self-renewal of MSCs [32,33], were upregulated in MSCs+PE (Fig. 3e). DNMT1, a major DNA methyltransferase responsible for maintaining methylation status during DNA replication, is directly regulated by OCT4 and NANOG [33]; its expression was also upregulated in MSCs+PE (Fig. 3e). Surprisingly, $p16^{INK4A}$ and $p14^{ARF}$, (*CDKN2A*) also increased mRNA expression in MSCs+PE, whereas expression of *p21(CDKN1A)*, *p53(TP53)*, and *RB1* decreased in MSCs+PE relative to donor-matched MSCs (Fig. 3f).

Human telomerase reverse transcriptase (TERT) is responsible for maintaining telomere length [34]. In the absence of TERT, the DNA replication complex cannot completely copy telomeric DNA; consequently, the telomeres shorten after each cell division. Cellular senescence and growth arrest are thought to occur when telomeres of one or more chromosomes reach a critical length [34]. The mRNA expression of *TERT* was higher in MSCs+PE than in untreated MSCs (Fig. 3g). *In situ* hybridisation analysis revealed higher expression of both *OCT4* and *CDKN2A* in MSCs+PE (Fig. S8), and the levels of *TERT* and *CDKN2A* were also increased (Fig. S8).

Hierarchical cluster analysis of genes that were differentially expressed in MSCs+PE *vs* untreated MSCs (Fig. 3h) revealed two major clusters, suggesting that $p14^{ARF}$ and $p16^{INK4A}$ are upregulated along with *OCT4*, *SOX2*, *NANOG*, *IDO1*, *TSG-6*, and *IL-6* (Cluster 1) rather than *p21*, *RB1*, *p53*, and alpha–smooth muscle actin (*α-SMA*; *ACTA2*) (Cluster 2; Fig. 3h). Principal component analysis showed that the MSC + PE group was located further from the cluster of continuous cultivation (CC) of MSCs (Fig. 3i). α-SMA also indicates an MSC fate associated with expression of F-actin (also known as stress fibers) mediated by translocation of YAP/TAZ transcription factors into the nucleus, a key event in regulation of genes associated with self-renewal and differentiation [35]. MSCs+PE decreased expression of F-actin (Fig. 3j and k) and nuclear localisation of YAP (Fig. 3j and l) while increasing their levels of phospho-YAP (Fig. 3m and n) and LATS1/2(Fig. 3m and o). Elevated expression of *CD47*, a key anti-phagocytic molecule, enables various types of cancer cells to evade phagocytosis by macrophages, thereby limiting programmed cell removal [36,37]. CD47 expression was reduced in MSCs+PE, as shown in Cluster 2 (Fig. 3h).

3.4. Functional senescent MSCs promote tissue remodelling in chronic inflammatory myopathy

In order to assess whether senescent MSC exert therapeutic effects by promoting the switch from the chronic inflammatory environment to regenerative acute inflammation, we transplanted senescent MSCs treated with PE, donor-matched MSCs, or PBS (vehicle control) into triceps surae of CIM mice (Fig. 4a). One day post-MSC transplantation, the percentage of $CD11b^+$ $F4/80^+$ macrophages did not differ among the three groups, whereas after 5 days the percentage of $CD11b^+$ $F4/80^+$ macrophages was higher in the MSC + PE group than in the MSC and vehicle groups (Fig. 4b and c). Furthermore, we could identify different patterns of macrophage phenotypes: the MSC and vehicle groups were enriched in anti-inflammatory $CD11b^+$ $F4/80^+$ $Ly6C^{low}$ macrophages, whereas the MSC + PE group was enriched in pro-inflammatory $CD11b^+$ $F4/80^+$ $Ly6C^{hi}$ macrophages 5 days post-transplantation (Fig. 4b and d). Interestingly, $F4/80^+$ macrophages accumulated close to $p16^{INK4A+}$ cells (Fig. 4e). Furthermore, the abundance of $CD11b^+$ $Gr\text{-}1^{hi}$ neutrophils transiently increased at 2 days post-transplantation only in the MSC + PE group (Fig. 4f and g), and $CD11b^+$ $Gr\text{-}1^{low}$

immature myeloid cells [38] were more abundant in MSCs+PE than in the vehicle control (Fig. 4f and h). We also examined $CD11b^+$ $CD49b^+$ NK cells by flow cytometry at 5 days post-transplantation. The MSC + PE group had a higher percentage of NK cells than the vehicle and MSC groups (Fig. 4i and j), and $CD49b^+$ NK cells accumulated near $p16^{INK4A+}$ cells in the MSC + PE group (Fig. 4k).

To determine whether $p16^{INK4A}$-expressing MSCs induce a regenerative inflammatory condition, we performed immunohistochemical staining for PDGFRα and $p16^{INK4A}$ in PKH-labelled transplanted MSCs. $p16^{INK4A}$-expressing $PDGFR\alpha^+$ FAPs were localised near PKH-labelled MSCs+PE on days 1 and 2 post–MSC transplantation (Fig. 5a). Interestingly, the PKH-labelled MSCs+PE did not express $p16^{INK4A}$ on day 2, whereas PKH-labelled MSC cells did (Fig. 5a). These results raised the possibility that $p16^{INK4A}$-expressing MSCs+PE could re-enter the cell cycle by downregulating $p16^{INK4A}$. To explore this idea, we passaged MSCs and MSCs+PE in normal media, and then subjected them to cell proliferation assays. MSCs+PE exhibited greater proliferative ability than MSCs (Fig. S9). At 5 days post- transplantation, PKH-labelled MSCs were not observed in any group, but high levels of $p16^{INK4A+}$ $PDGFR\alpha^+$ FAPs were observed only in MSCs+PE (Fig. 5a). In these mice, serial sections revealed infiltration of the transplanted area by macrophages and NK cells (Fig. 5a and Fig. 4e and k). In addition, we evaluated regeneration of myofibers, and observed that the central nuclei and cross-sectional area of each myofiber were improved in the MSC + PE group relative to the vehicle and MSC groups (Fig. 5b–5e). Moreover, hind limb grip strength (an indicator of muscle function) was greater in MSC + PE–transplanted muscle at 13 days post-transplantation (Fig. 5f).

These results raised the possibility that transplanted MSCs+PE could induce senescence in FAPs and promote muscle remodelling. To explore this idea, we performed proteome array analysis to determine which cytokines were secreted from MSCs+PE (Fig. S10). Levels of DPP-4, a surface protein that is abundant in senescent cells and enables their preferential elimination [31], and SerpinE1 (plasminogen activator inhibitor 1[PAI-1]), a major component of the SASP [39], were elevated in MSCs+PE (Fig. S10). We then sought to determine whether SASP factors secreted by MSCs+PE induced FAPs senescence. To this end, we cultured FAPs with culture supernatant of MSCs+PE. In-cell ELISA analysis revealed that factors secreted by MSCs+PE promoted $p16^{INK4A}$ expression in FAPs; in addition, the DPP-4 inhibitor vildagliptin and neutralising antibodies against SerpinE1 (PAI-1) decreased $p16^{INK4A}$ expression of FAPs (Fig. S11). YKL-40 (chitinase 3-like-1 [CHI3L1]) was also upregulated by MSCs+PE supernatant. YKL-40 up-regulates two pro-inflammatory mediators, C-chemokine ligand 2 (CCL2) and chemokine CX motif ligand 2 (CXCL2), which promote remodelling in acute skeletal muscle injury [40]; both of these proteins were also upregulated in MSCs+PE (Fig. S10).

Further, to determine whether senescent MSCs+PE were phagocytosed more often than MSC, we performed phagocytosis assays by co-culturing MSCs+PE or MSCs with RAW264.7 cells *in vitro*. MSCs and MSCs+PE were labelled using PKH26, and RAW264.7 macrophages were labelled with PKH2. Co-culture was performed in complete medium for a total of 72 h. Cells engulfing PKH26-positive cells were identified as PKH2-labelled RAW264.7 macrophages, and the percentage of $PKH2^+$ $PKH26^+$ cells increased in coculture of MSCs+PE and RAW264.7 macrophages, suggesting that phagocytosis was more active in the MSC + PE cultures (Fig. S12).

3.5. CDKN2A expression in MSCs is required to induce regenerative inflammation for treatment of chronic inflammatory myopathy

We next sought to determine whether expression of *CDKN2A* (the locus that encodes INK4A and ARF) [41] in MSCs treated with PE would influence the therapeutic effects of these cells. Using the CRISPR/Cas9 system, we created GFP-labelled *CDKN2A* knockout (KO) or scrambled control (SC) MSCs, incubated them in PE-containing media (Fig. S2), and transplanted the cells into the triceps surae of CIM mice (Fig. 6a). The proportions of GFP^+ engrafted cells were 3.2% (KO-MSC) and 2.2% (SC-MSC) at 1 day after transplantation, but the abundance of SC-MSCs increased transiently at 2 days after transplantation (to 10%), and subsequently decreased with time (Fig. 6b and c). We observed an increase in $CD11b^+$ $Gr\text{-}1^{hi}$ neutrophils at day 2 after SC-MSC transplantation, followed by a decrease on day 5; by contrast, in the KO-MSC transplantation, no increase in neutrophil abundance was observed at any time point (Fig. S13). The abundance of $CD11b^+$ $Gr\text{-}1^{low}$ monocytes also increased at day 1 after SC-MSC transplantation and decreased on day 2. By contrast, in the KO-MSC transplantation, no increase in $CD11b^+$ $Gr\text{-}1^{low}$ monocytes was observed at any time point (Fig. S13). The abundance of $CD11b^+$ $F4/80^+$ macrophages increased on day 1 after SC-MSC transplantation and decreased by day 11, and we could detect cellular switching from $CD11b^+$ $F4/80^+$ $Ly6C^{hi}$ pro-inflammatory macrophages to $CD11b^+$ $F4/80^+$ $Ly6C^{low}$ anti-inflammatory macrophages at this time point (Fig. 6d–6f). By contrast, KO-MSC–transplanted muscle predominantly contained anti-inflammatory macrophages and lacked cells in the inflammatory phase (Fig. 6d–6f). The percentage of CD45-CD31-$Integrin\alpha7^+$ satellite cells was smaller in KO-MSC–transplanted than in SC-MSC–transplanted muscle (Fig. 6g and h), and KO-MSC had a comparatively weak therapeutic effect on muscle cross-sectional area (Fig. 6i and j).

4. Discussion

Despite the widespread clinical use of MSCs, their therapeutic mechanism remains largely unresolved, and this gap in our knowledge may explain why the results of clinical trials using these cells have often been controversial. Here, we showed that $p16^{INK4A}$-expressing MSCs promote regenerative processes in chronic inflammatory myopathy by inducing infiltration of immune cells, especially phagocytes, with distinct temporal and spatial kinetics over the course of inflammation. The therapeutic efficacy of senescent MSCs may explain the paradoxical observation that MSCs are therapeutically efficacious despite their lack of engraftment.

Cellular senescence, which is induced by a complex stress response, causes cells that are capable of proliferating to lose this ability in many biological and pathological settings [39]. The senescence response is implicated in two apparently disparate processes: tumour suppression and chronic inflammation/fibrosis. Several lines of evidence indicate that oncogene-induced senescence functions as a tumourigenesis barrier during early stages of tumourigenesis [42]. In addition, cellular senescence also limits the fibrogenic response to tissue damage by facilitating the clearance of senescent cells by phagocytosis [10]. Removal of senescent cells attenuates the development of fibrosis and creates a pro-regenerative environment [39]. We demonstrated that in contrast to normal tissue, senescent FAPs were less abundant in chronic inflammation than in acute inflammation, and that local injection of $p16^{INK4A\text{-}hi}$ MSCs into CIM mice promotes FAP senescence and infiltration of immune cells with a phagocytotic phenotype that induces regenerative inflammation. Anti-senescent therapeutics, termed senolytics, already exist [43]. Both anti-senescence therapy and our pro-senescence therapy aim to deplete senescent cells with the goal of promoting regeneration. Pro-senescence therapy could cause potent senescence in a chronic inflammatory environment, like the remodelling process of acute inflammation, which induces the tissue's innate repair process.

Recent studies have identified a beneficial effect of senescent cells, especially $p16^{INK4A}$-expressing cells [10,15,44,45]. $p16^{INK4A}$ prevents cell cycle progression from G1 to S phase by inhibiting two cycle-dependent kinases, CDK4 and CDK6 [46]. $p16^{INK4A}$-positive fibroblasts and endothelial cells appear very early in response to a cutaneous wound [15] and accelerate cutaneous wound healing *via* induction of CYR61 (cysteine-rich protein 61) [14]. In the liver, cellular senescence limits the extent of fibrosis following liver damage, facilitating clearance

of senescent cells by NK cells [10]; moreover, CDKN2A induced by muscle damage positively correlates with *in vivo* reprogramming mediated by IL-6, a major component of the SASP [45]. Our data support the idea that cellular senescence, especially $p16^{INK4A}$, promotes remodelling after injury. Intriguingly, in this study, $p16^{INK4A}$-expressing FAPs were more abundant 1 or 2 days after transplantation of MSCs+PE, and most of these cells were located near engrafted MSCs. This process, mediated by paracrine transmission of cellular senescence, has been termed "bystander senescence" [47,48]. In addition, $p16^{INK4A}$-expressing FAPs were present in regions where engrafted MSCs did not exist 5 days after transplantation of MSCs+PE, suggesting that bystander senescence might have spread after the transplanted MSCs were eliminated. We found that the senescence-related factor DPP-4 was secreted into the culture supernatant at higher levels by MSCs+PE than by non-treated MSCs. DPP-4 (also known as CD26) is much more abundant in senescent cells, and selective expression of DPP-4 on the surface of senescent cells promotes their preferential elimination by NK cells [31]. DPP-4 is likely to be only one of the factors present in PE, but it clearly has the ability to induce senescence in MSCs.

A major impact of our study is the identification of an effective MSC subpopulation, based on the remodelling mechanism of chronic inflammatory myopathy. Although induction of $p16^{INK4A\text{-}hi}$ MSCs is important for therapeutic activity, functional senescence may be distinct from senescence that occurs due to continuous cultivation, UV exposure, oxidative stress, or heat shock [29]. Indeed, $p16^{INK4A}$ in MSCs is also upregulated by long-term culture or other culture conditions. In such cases, the cells typically become enlarged and flattened, and downregulate genes related to differentiation, cytoskeletal maintenance, and mitochondrial function; this attenuates their therapeutic efficacy against fibrotic tissue [29].

Our study demonstrated that transplantation of MSCs+PE into CIM muscle can activate phagocytosis, followed by tissue repair. Specifically, senescent MSCs+PE shift the dominant phenotype of macrophages from anti-inflammatory to pro-inflammatory; subsequently, anti-inflammatory macrophages became dominant again, resulting in tissue repair. Most chronic inflammatory diseases have refractory fibrosis due to the predominance of anti-inflammatory macrophages, and the conversion from the anti-inflammatory to pro-inflammatory phenotype may aid in removal of fibrosis or cancer-related cells [49]. Transplantation of MSCs+PE enhanced phagocytic activity by activating pro-inflammatory macrophages, NK cells, and Gr-1^{hi} neutrophils, followed by a decrease in the abundance of pro-inflammatory macrophages and NK cells and an increase in the potent suppressive activity of Gr-1^{low} immature myeloid cells against $CD8^+$ T cells [50]. This might promote remodelling in this chronic myopathy model, in which infiltration by $CD8^+$ cells is predominant [19]. *CDKN2A*-KO MSCs did not exhibit these immune-activating effects even when cultured in PE-containing medium. These results provide evidence that *CDKN2A* expression in MSCs is essential for treatment of CIM by creation of a regenerative inflammatory state.

We used human MSCs to understand the cell-biological reaction of human MSCs to human placental extracts. Certainly, the effect of (and response to) xenotransplantation of MSCs may differ from that of transplantation of allogenic or autogenic MSCs [51]. However, Galleu et al. reported that the results of treating GvHD patients with human MSCs were similar to those of treating a GvHD mouse model with human MSCs, and that mouse inflammatory cytokines did not activate immunomodulatory molecules (IDO, TSG-6 or PTSG2 [prostaglandin-endoperoxide synthase 2]) in human MSCs [6]. Therefore, in order to evaluate the therapeutic potential of human MSCs for future clinical therapeutic applications, we performed this study using human MSCs.

This study highlights a new strategy for MSC treatment based on senescence-induced regeneration. A further impact of our discovery is that the pertinent senescent MSC population provides a powerful therapeutic effect, mediated by the creation of a regenerative inflammatory state, in a murine CIM model. Like muscle tissue, most tissues in the body contain resident mesenchymal cells and resident or infiltrated immune cells; therefore, the principle underpinning this therapeutic mechanism should be applicable to other chronic inflammatory diseases. The intriguing potential of senescent MSCs may provide new opportunities for the clinical application of these cells.

Acknowledgements/Funding

The authors would like to thank Ms. Kozue Kamiya, Ms. Yuko Hayakawa, and Mr. Tatsuya Shiraishi for their technical support, as well as Zenis Co. Ltd. for providing native language editing services. This work supported by Medical Research Grant in Sapporo Medical University and JSPS KAKENHI Grant Number JP16K16430. The funder had no role in study design, data collection, data analysis, interpretation, or writing of the report.

Takako S. Chikenji (corresponding author) had full access to all the data in the study and had final responsibility for the decision to submit for publication.

Funding

Medical Research Grant in Sapporo Medical University and JSPS KAKENHI Grant Number JP16K16430.

Declaration of interests

The authors declare no competing interests associated with this manuscript.

Author contributions

T.C. Y.S. designed all of the studies. T.C., Y.S., N.K., M.N., Y.M., and M.O. conducted all experiments. T.C. and Y.S. performed data analysis. T.C., Y.S., and M.F. contributed to drafting and review of the manuscript.

Appendix A. Supplementary data

Supplementary data to this article can be found online at https://doi.org/10.1016/j.ebiom.2019.05.012.

References

[1] Ankrum JA, Ong JF, Karp JM. Mesenchymal stem cells: immune evasive, not immune privileged. Nat Biotechnol 2014;32:252–60. https://doi.org/10.1038/nbt.2816.
[2] Bianco P, Cao X, Frenette PS, Mao JJ, Robey PG, Simmons PJ, et al. The meaning, the sense and the significance: translating the science of mesenchymal stem cells into medicine. Nat Med 2013;19:35–42. https://doi.org/10.1038/nm.3028.
[3] Bernardo ME, Fibbe WE. Mesenchymal stromal cells: sensors and switchers of inflammation. Cell Stem Cell 2013;13:392–402. https://doi.org/10.1016/j.stem.2013.09.006.
[4] Melief SM, Schrama E, Brugman MH, Tiemessen MM, Hoogduijn MJ, Fibbe WE, et al. Multipotent stromal cells induce human regulatory T cells through a novel pathway involving skewing of monocytes toward anti-inflammatory macrophages. Stem Cells 2013;31:1980–91. https://doi.org/10.1002/stem.1432.
[5] Németh K, Leelahavanichkul A, Yuen PST, Mayer B, Parmelee A, Doi K, et al. Bone marrow stromal cells attenuate sepsis via prostaglandin E2–dependent reprogramming of host macrophages to increase their interleukin-10 production. Nat Med 2008;15:42–9. https://doi.org/10.1038/nm.1905.
[6] Galleu A, Riffo-Vasquez Y, Trento C, Lomas C, Dolcetti L, Cheung TS, et al. Apoptosis in mesenchymal stromal cells induces in vivo recipient-mediated immunomodulation. Sci Transl Med 2017;9:eaam7828. https://doi.org/10.1126/scitranslmed.aam7828.
[7] Vriz S, Reiter S, Galliot B. Cell death a program to regenerate. Curr Top Dev Biol 2014;108:121–51. https://doi.org/10.1016/B978-0-12-391498-9.00002-4.
[8] Lemos DR, Babaeijandaghi F, Low M, Chang C-K, Lee ST, Fiore D, et al. Nilotinib reduces muscle fibrosis in chronic muscle injury by promoting TNF-mediated apoptosis of fibro/adipogenic progenitors. Nat Med 2015;21:786–94. https://doi.org/10.1038/nm.3869.
[9] Childs BG, Baker DJ, Kirkland JL, Campisi J, van Deursen JM. Senescence and apoptosis: dueling or complementary cell fates? EMBO Rep 2014;15:1139–53. https://doi.org/10.15252/embr.201439245.

[10] Krizhanovsky V, Yon M, Dickins RA, Hearn S, Simon J, Miething C, et al. Senescence of activated stellate cells limits liver fibrosis. Cell 2008;134:657–67. https://doi.org/10.1016/j.cell.2008.06.049.
[11] He S, Sharpless NE. Senescence in health and disease. Cell 2017;169:1000–11. https://doi.org/10.1016/j.cell.2017.05.015.
[12] Krishnamurthy J, Torrice C, Ramsey MR, Kovalev GI, Al-Regaiey K, Su L, et al. Ink4a/Arf expression is a biomarker of aging. J Clin Invest 2004;114:1299–307. https://doi.org/10.1172/JCI22475.
[13] Ressler S, Bartkova J, Niederegger H, Bartek J, Scharffetter-Kochanek K, Jansen-Dürr P, et al. p16INK4A is a robust in vivo biomarker of cellular aging in human skin. Aging Cell 2006;5:379–89. https://doi.org/10.1111/j.1474-9726.2006.00231.x.
[14] Jun J-I, Lau LF. The matricellular protein CCN1 induces fibroblast senescence and restricts fibrosis in cutaneous wound healing. Nat Cell Biol 2010;12:676–85. https://doi.org/10.1038/ncb2070.
[15] Demaria M, Ohtani N, Youssef SA, Rodier F, Toussaint W, Mitchell JR, et al. An essential role for senescent cells in optimal wound healing through secretion of PDGF-AA. Dev Cell 2014;31:722–33. https://doi.org/10.1016/j.devcel.2014.11.012.
[16] Sturmlechner I, Durik M, Sieben CJ, Baker DJ, van Deursen JM. Cellular senescence in renal ageing and disease. Nat Rev Nephrol 2016;13:77–89. https://doi.org/10.1038/nrneph.2016.183.
[17] Dalakas MC. Inflammatory muscle diseases. N Engl J Med 2015;372:1734–47. https://doi.org/10.1056/NEJMra1402225.
[18] Hardy D, Besnard A, Latil M, Jouvion G, Briand D, Thépenier C, et al. Comparative study of injury models for studying muscle regeneration in mice. PLoS One 2016;11. https://doi.org/10.1371/journal.pone.0147198 (e0147198).
[19] Allenbach Y, Solly S, Grégoire S, Dubourg O, Salomon B, Butler-Browne G, et al. Role of regulatory T cells in a new mouse model of experimental autoimmune myositis. Am J Pathol 2009;174:989–98. https://doi.org/10.2353/ajpath.2009.080422.
[20] Kamala T. Hock immunization: a humane alternative to mouse footpad injections. J Immunol Methods 2007;328:204–14. https://doi.org/10.1016/j.jim.2007.08.004.
[21] Kanda Y. Investigation of the freely available easy-to-use software "EZR" for medical statistics. vol. 48. 2013. doi:https://doi.org/10.1038/bmt.2012.244.
[22] Bentzinger CF, Wang YX, Dumont NA, Rudnicki MA. Cellular dynamics in the muscle satellite cell niche. EMBO Rep 2013;14:1062–72. https://doi.org/10.1038/embor.2013.182.
[23] Blau HM, Cosgrove BD, Ho ATV. The central role of muscle stem cells in regenerative failure with aging. Nat Med 2015;21:854–62. https://doi.org/10.1038/nm.3918.
[24] Summan M, Warren GL, Mercer RR, Chapman R, Hulderman T, van Rooijen N, et al. Macrophages and skeletal muscle regeneration: a clodronate-containing liposome depletion study. Am J Phys Regul Integr Comp Phys 2006;290:R1488–95. https://doi.org/10.1152/ajpregu.00465.2005.
[25] Mounier R, Théret M, Arnold L, Cuvellier S, Bultot L, Göransson O, et al. AMPKα1 regulates macrophage skewing at the time of resolution of inflammation during skeletal muscle regeneration. Cell Metab 2013;18:251–64. https://doi.org/10.1016/j.cmet.2013.06.017.
[26] Vidal B, Serrano AL, Tjwa M, Suelves M, Ardite E, De Mori R, et al. Fibrinogen drives dystrophic muscle fibrosis via a TGFbeta/alternative macrophage activation pathway. Genes Dev 2008;22:1747–52. https://doi.org/10.1101/gad.465908.
[27] Cudejko C, Wouters K, Fuentes L, Hannou SA, Paquet C, Bantubungi K, et al. p16INK4a deficiency promotes IL-4-induced polarization and inhibits proinflammatory signaling in macrophages. Blood 2011;118:2556–66. https://doi.org/10.1182/blood-2010-10-313106.
[28] Bonab MM, Alimoghaddam K, Talebian F, Ghaffari SH, Ghavamzadeh A, Nikbin B. Aging of mesenchymal stem cell in vitro. BMC Cell Biol 2006;7:14. https://doi.org/10.1186/1471-2121-7-14.
[29] Turinetto V, Vitale E, Giachino C. Senescence in human mesenchymal stem cells: functional changes and implications in stem cell-based therapy. Int J Mol Sci 2016;17. https://doi.org/10.3390/ijms17071164.
[30] Chuprin A, Gal H, Biron-Shental T, Biran A, Amiel A, Rozenblatt S, et al. Cell fusion induced by ERVWE1 or measles virus causes cellular senescence. Genes Dev 2013;27:2356–66. https://doi.org/10.1101/gad.227512.113.
[31] Kim KM, Noh JH, Bodogai M, Martindale JL, Yang X, Indig FE, et al. Identification of senescent cell surface targetable protein DPP4. Genes Dev 2017;31:1529–34. https://doi.org/10.1101/gad.302570.117.
[32] Seo E, Basu-Roy U, Gunaratne PH, Coarfa C, Lim D-S, Basilico C, et al. SOX2 regulates YAP1 to maintain Stemness and determine cell fate in the Osteo-Adipo lineage. CellReports 2013;3:2075–87. https://doi.org/10.1016/j.celrep.2013.05.029.
[33] Tsai C-C, Su P-F, Huang Y-F, Yew T-L, Hung S-C. Oct4 and Nanog directly regulate Dnmt1 to maintain self-renewal and undifferentiated state in mesenchymal stem cells. Mol Cell 2012;47:169–82. https://doi.org/10.1016/j.molcel.2012.06.020.
[34] Simonsen JL, Rosada C, Serakinci N, Justesen J, Stenderup K, Rattan SIS, et al. Telomerase expression extends the proliferative life-span and maintains the osteogenic potential of human bone marrow stromal cells. Nat Biotechnol 2002;20:592–6. https://doi.org/10.1038/nbt0602-592.
[35] Talele NP, Fradette J, Davies JE, Kapus A, Hinz B. Expression of α-smooth muscle actin determines the fate of mesenchymal stromal cells. Stem Cell Reports 2015;4:1016–30. https://doi.org/10.1016/j.stemcr.2015.05.004.
[36] Majeti R, Chao MP, Alizadeh AA, Pang WW, Jaiswal S, Gibbs KD, et al. CD47 is an adverse prognostic factor and therapeutic antibody target on human acute myeloid leukemia stem cells. Cell 2009;138:286–99. https://doi.org/10.1016/j.cell.2009.05.045.
[37] Chao MP, Majeti R, Weissman IL. Programmed cell removal: a new obstacle in the road to developing cancer. Nat Rev Cancer 2011;12:58–67. https://doi.org/10.1038/nrc3171.
[38] Tsiganov EN, Verbina EM, Radaeva TV, Sosunov VV, Kosmiadi GA, Nikitina IY, et al. Gr-1dimCD11b+ immature myeloid-derived suppressor cells but not neutrophils are markers of lethal tuberculosis infection in mice. J Immunol 2014;192:4718–27. https://doi.org/10.4049/jimmunol.1301365.
[39] Muñoz-Espín D, Serrano M. Cellular senescence: from physiology to pathology. Nat Rev Mol Cell Biol 2014;15:482–96. https://doi.org/10.1038/nrm3823.
[40] Lu H, Huang D, Ransohoff RM, Zhou L. Acute skeletal muscle injury: CCL2 expression by both monocytes and injured muscle is required for repair. FASEB J 2011;25:3344–55. https://doi.org/10.1096/fj.10-178939.
[41] Popov N, Gil J. Epigenetic regulation of the INK4b-ARF-INK4a locus: in sickness and in health. Epigenetics 2010;5:685–90. https://doi.org/10.4161/epi.5.8.12996.
[42] Prieur A, Peeper DS. Cellular senescence in vivo: a barrier to tumorigenesis. Curr Opin Cell Biol 2008;20:150–5. https://doi.org/10.1016/j.ceb.2008.01.007.
[43] Kirkland JL, Tchkonia T, Zhu Y, Niedernhofer LJ, Robbins PD. The clinical potential of Senolytic drugs. J Am Geriatr Soc 2017;65:2297–301. https://doi.org/10.1111/jgs.14969.
[44] Helman A, Klochendler A, Azazmeh N, Gabai Y, Horwitz E, Anzi S, et al. p16Ink4a-induced senescence of pancreatic beta cells enhances insulin secretion. Nat Med 2016;22:412–20. https://doi.org/10.1038/nm.4054.
[45] Chiche A, Le Roux I, Joest von M, Sakai H, Aguín SB, Cazin C, et al. Injury-induced senescence enables in vivo reprogramming in skeletal muscle. Cell Stem Cell 2017;20:407–414.e4. https://doi.org/10.1016/j.stem.2016.11.020.
[46] Sherr CJ, Roberts JM. CDK inhibitors: positive and negative regulators of G1-phase progression. Genes Dev 1999;13:1501–12. https://doi.org/10.1038/35036002.
[47] Tasdemir N, Lowe SW. Senescent cells spread the word: non-cell autonomous propagation of cellular senescence. EMBO J 2013;32:1975–6. https://doi.org/10.1038/emboj.2013.139.
[48] Acosta JC, Banito A, Wuestefeld T, Georgilis A, Janich P, Morton JP, et al. A complex secretory program orchestrated by the inflammasome controls paracrine senescence. Nat Cell Biol 2013;15:978–90. https://doi.org/10.1038/ncb2784.
[49] Das A, Sinha M, Datta S, Abas M, Chaffee S, Sen CK, et al. Monocyte and macrophage plasticity in tissue repair and regeneration. Am J Pathol 2015;185:2596–606. https://doi.org/10.1016/j.ajpath.2015.06.001.
[50] Youn J-I, Gabrilovich DI. The biology of myeloid-derived suppressor cells: the blessing and the curse of morphological and functional heterogeneity. Eur J Immunol 2010;40:2969–75. https://doi.org/10.1002/eji.201040895.
[51] Galipeau J, Sensebé L. Mesenchymal stromal cells: clinical challenges and therapeutic opportunities. Cell Stem Cell 2018;22:824–33. https://doi.org/10.1016/j.stem.2018.05.004.